Synchronization and Collective Behavior in Globally Coupled Logarithmic Maps

M. G. Cosenza and J. González
Centro de Astrofísica Teórica, Facultad de Ciencias, Universidad de Los Andes,
A. Postal 26 La Hechicera, Mérida 5251, Venezuela
(submitted to Phys. Rev. E, 1997)

The phenomena of synchronization and nontrivial collective behavior in a system of globally coupled chaotic logarithmic maps are investigated through the properties of the mean field of the network. Several collective states are found in the phase diagram of the system: synchronized, collective periodic, collective chaotic, and fully turbulent states. In contrast with other globally coupled systems, no clustering nor quasiperiodic collective states occur in this model. The organization of the observed nontrivial collective states is related to the presence of unstable periodic orbits in the local dynamics.

PACS Numbers 05.45.+b, 02.50.-r

I. INTRODUCTION.

Coupled map lattices (CML) are discrete space, discrete time dynamical systems of interacting elements whose states vary continuously according to specific functions. Globally coupled maps constitute a class of CML where the coupling interaction is a function of all the elements [1]. Though CML models are idealized systems, they have proved capable of capturing much of the phenomenology observed in a variety of complex spatiotemporal processes, with the advantage of being computationally efficient and, in many cases, mathematically tractable [2].

There has been recent interest in the use of CML models in the investigation of cooperative phenomena, such as synchronization or nontrivial collective behavior, which appear in many extended chaotic dynamical systems [3–7]. Synchronization consists in the complete coincidence in time of the states of the elements in a system, while nontrivial collective behavior is characterized by a well-defined temporal evolution of statistical quantities emerging out of local chaos.

An important category of systems with many degrees of freedom which can exhibit these collective effects are globally coupled nonlinear oscillators. Such systems arise naturally in the description of Josephson junctions arrays, charge density waves, multimode lasers, neural dynamics, ecological and evolution models [8–12]. Globally coupled maps represent a useful approach to the study of many processes on this kind of systems, in particular to the search of the conditions for the occurrence of collective dynamics.

Studies in globally coupled chaotic maps have revealed interesting features such as a) formation of clusters, i.e., differentiated subsets of synchronized elements within the network [13]; b) non-statistical properties in the fluctuations of the mean field of the ensemble [13,14]; c) global quasiperiodic motion [15,16]; and different collective phases depending on the parameters of the system [15,17]. These works have considered mainly bounded or unimodal maps belonging to some universality class (quadratic, circle or tent maps) as the source of local chaos.

In this article, we investigate the phenomena of synchronization and nontrivial collective behavior in globally coupled systems by using unbounded chaotic elements and whose properties differ from those of previously used maps in the same context. The local dynamics that we employ is the logarithmic map introduced by Kawabe and Kondo [18] and which has shown to produce collective behavior with period two on locally coupled map lattices [19]. Our model of globally coupled logarithmic maps provides a situation to examine the role that different local dynamics play on the emergence and universality of the various types of collective behavior in globally coupled systems. In addition, the unbounded character of the local functions places no restrictions on the range of the parameters of the system that can be explored.

In section II we define the model and show the properties of the local logarithmic map. In section III the synchronized states of the network are studied. The collective states arising from desynchronized local maps are investigated on the phase diagram of the system in section IV. Some differences occur in comparison to previously studied globally coupled systems, for example, no clustering and no quasiperiodic collective behavior appear to take place in our model. The influence of the size of the system on the emergence of collective states is calculated in Section V. The results are discussed in section VI.

II. GLOBALLY COUPLED LOGARITHMIC MAPS.

We consider the globally coupled map system

$$x_{t+1}(i) = (1-\epsilon) f(x_t(i)) + \frac{\epsilon}{N} \sum_{j=1}^{N} f(x_t(j)), \tag{1}$$

where $x_t(i)$ gives the state of the lattice element i ($i = 1, \ldots, , N$ = system size) at a discrete time step t, ϵ is the coupling parameter, and f is a map defining the local dynamics.

The collective behavior of the globally coupled maps can be described through the instantaneous mean field of the system, defined as

$$h_t = \frac{1}{N} \sum_{j=1}^{N} f(x_t(j)). \tag{2}$$

The local dynamics corresponds to the logarithmic map [18],

$$x_{t+1} = f(x_t) = b + \ln |x_t| \,, \tag{3}$$

where b is a real parameter. This map does not belong to the standard classes of universality of unimodal or bounded maps. It possesses no maximum or minimum and its Schwarzian derivative is always positive. Figure 1 shows the bifurcation diagram of the iterates of the logarithmic map as a function of the parameter b. Two stable fixed points satisfying $f(x^*) = x^*$ and $|f'(x^*)| < 1$ exist for this map: $x_1^* < -1$, for $b < -1$; and $x_2^* > 1$, for $b > 1$; both are indicated in fig. 1. Chaos occurs in the parameter interval $b \in [-1, 1]$. Figure 1 reveals the absence of separated chaotic bands at any given value of $b \in [-1, 1]$. The fixed point x_1^* becomes unstable at $b = -1$, giving rise to chaos via type III intermittency associated to an inverse period doubling bifurcation. The stable fixed point x_2^* originates from a tangent bifurcation at $b = 1$, and the transition to chaos at this value of b takes place through type I intermittency. There exist several unstable period-m orbits $\bar{x}$ satisfying $f^{(m)}(\bar{x}) = \bar{x}$ in the chaotic range $b \in [-1, 1]$. Figure 2 shows some unstable periodic orbits of the logarithmic map as a function of the parameter b.

Figure 3 shows the Lyapunov exponent λ of the logarithmic map as a function of the parameter b. Note that λ is positive on the whole region $b \in [-1, 1]$ and thus no periodic windows appear in any subinterval of b in the chaotic region. The logarithmic map Eq. (3) belongs to a class of singular chaotic maps characterized by having positive Schwarzian derivative, unbounded dynamics, and by the absence of periodic windows in the chaotic interval of their parameters [20].

III. SYNCHRONIZATION

The coupled map system (1) can be expressed in vector form as

$$\mathbf{x}_{t+1} = \left[(1-\epsilon)\mathbf{I} + \frac{\epsilon}{N}\mathbf{M} \right] \mathbf{f}(\mathbf{x}_t), \tag{4}$$

where the N-dimensional vectors $\mathbf{x}_t$ and $\mathbf{f}(\mathbf{x}_t)$ have components $[\mathbf{x}_t]_i = x_t(i)$ and $[\mathbf{f}(\mathbf{x}_t)]_i = f(x_t(i))$, respectively; $\mathbf{M}$ is an $N \times N$ matrix with all its components being equal to 1; and $\mathbf{I}$ is the $N \times N$ identity matrix.

The simplest kind of global attractor in the system Eq. (4) is the synchronized state, with $x_t(i) = x_t(j)\ \forall\ i, j$, in which case the dynamics is described just by the single logarithmic map $x_{t+1} = f(x_t)$.

From the linear stability analysis of synchronized states in coupled map lattices, it can be shown that these states are stable if the following condition is satisfied [1,21]

$$\left| \left(1 - \epsilon + \frac{\epsilon}{N} \mu_k \right) e^{\lambda} \right| < 1, \tag{5}$$

where $\{\mu_k : \ k = 1, \ldots, N\}$ is the set of eigenvalues of the coupling matrix $\mathbf{M}$ and λ is the Lyapunov exponent of the single logarithmic map (fig. 3). In the globally coupled case, the eigenvalues are $\mu_k = 0$ ($k = 1, 2, \ldots, N-1$) which has (N-1)-fold degeneracy and $\mu_N = N$. Because of these eivenvalues, the synchronization condition is independent of N, i.e., it can be achieved with any number of globally coupled maps. The eigenvectors of the matrix $\mathbf{M}$ constitute

a complete basis on which any state $\mathbf{x}_t$ of the system can be expressed as a linear combination. The eigenvector corresponding to the eigenvalue $\mu_N = N$ is the homogeneous one; thus perturbations of the state $\mathbf{x}_t$ along this eigenvector do not destroy the coherence, and the stability condition associated to $\mu_N = N$ is irrelevant for a synchronized state. The other $(N-1)$ eigenvectors associated to $\mu_k = 0$ are not homogeneous. Thus, condition (5) with $\mu_k = 0$ defines a region on the space of parameters (b, ϵ) of the system (4) where all the stable synchronized states can be observed.

Two types of stable synchronized states satisfying condition (5) are found in the system of globally coupled logarithmic maps:

1) *synchronized stationary states*, for which $x_t(i) = x_1^*$ for $b < -1$, and $x_t(i) = x_2^*$ for $b > 1$, $\forall i$, corresponding to constant values of the mean field. The boundaries of the stability regions of the synchronized stationary states are given by

$$\left(1 - \epsilon + \frac{\epsilon}{N}\mu_k\right) |f'(x_{1,2}^*)| = \pm 1. \tag{6}$$

Equations (6) yield curves in the parameter plane (b, ϵ) which determine where each coherent stationary state exists. Figure 4 shows the stability boundaries of each of these states, with $b < -1$ and $b > 1$, respectively, corresponding to the eigenvalues $\mu_k = 0$ and $\mu_N = N$. Inside these regions of stable synchronized stationary states, the mean field takes the values $h_t = x_1^*$, for $b < -1$, and $h_t = x_2^*$, for $b > 1$. Note that synchronization can occur for all values of the coupling in the phase diagram of the system since the local dynamics is unbounded.

2) *synchronized chaotic state*, for which $x_t(i) = f(x_t)$, $\forall i$, in the parameter range $b \in [-1, 1]$. The stability region of this state is bounded by the curves

$$\left(1 - \epsilon + \frac{\epsilon}{N}\mu_k\right) e^{\lambda} = \pm 1, \tag{7}$$

with $\lambda(b)$ calculated in fig. 2. Figure 4 shows the boundaries given by Eq.(7) with $\mu_k = 0$. The curves corresponding to the eigenvalue $\mu_n = N$ reduce to $b = -1$ and $b = 1$ in both, Eq. (6) and Eq. (7). These values of b separate the synchronized chaotic state $h_t = f(x_t)$ from the synchronized stationary states $h_t = x_1^*$ and $h_t = x_2^*$. In either region of synchronized states, the globally coupled system, Eq. (4), forms a stable single cluster, which has been verified by direct simulations with random initial conditions.

The global coupling induces different degrees of synchronization in the network, depending on the proximity of the parameter ϵ to its values on the synchronization boundaries. The synchronization of the lattice can be characterized by the the time-average $\langle\sigma\rangle$ of the instantaneous standard deviations σ_t of the distribution of site variables $x_t(i)$, defined as

$$\sigma_t = \left(\frac{1}{N}\sum_{i=1}^{N} \left[f\left(x_t(i)\right) - h_t\right]^2\right)^{1/2}. \tag{8}$$

Figure 5 shows the quantity $\langle\sigma\rangle$ as a function of the coupling parameter ϵ, with fixed $b = -0.7$, calculated after discarding the transients and starting from random initial conditions on the local maps for each value of ϵ. Within the synchronization region, $\langle\sigma\rangle$ reaches its minimum value, very close to zero. Perfect synchronization, i.e. $\langle\sigma\rangle \equiv 0$, is limited by the finite precision of the calculations. The "amount" of synchronization decreases with increasing distance from the synchronization boundaries. Figure 5 also shows the location of the collective states associated to desynchronization in the system, which are discussed in the next section.

IV. DESYNCHRONIZED STATES.

The crossing of the synchronization boundaries with $\mu_k = 0$ in fig. 4 marks the appearance of desynchronized states for which $x_t(i) \neq x_t(j)$. In order to investigate the collective dynamics of the system (4) in different regions of its parameter space (b, ϵ) outside the synchronization zone, we have constructed bifurcation diagrams of the asymptotic mean field h_t as a function of the parameters. Note that this system allows any real values of b and ϵ. Negative values of ϵ may represent some physical situations, which have also been studied with CML models [22,23].

We have observed desynchronized states with different types of collective temporal manifestations, existing in different regions of the phase diagram, fig. 4. These states consist of: a) *collective periodic behavior*, b) *collective chaotic bands*, and c) *full turbulence*.

a) Collective periodic behavior.

When the parameter b is in the range $[-1, 1]$, the elements $x_t(i)$ are chaotic and desynchronized. However, the mean field of the system reveals the existence of global periodic attractors. Figures 6(a) and 6(b) display the bifurcation diagrams h_t vs b for two different fixed values of the coupling parameter ϵ. For each value of b, the mean field was calculated at each time step during a run starting from random initial conditions on the local maps, uniformly distributed on the interval $[-8, 4]$, after discarding the transients. In this representation, collective periodic states at a given value of the parameter b appear as sets of vertical segments which correspond to intrinsic fluctuations of the periodic orbits of the mean field.

For small values of the coupling ϵ, fig. 6(a) shows simple periodic collective states occurring in the chaotic range of the local dynamics: a pitchfork bifurcation takes place from a collective fixed point (a state for which the time series of h_t statistically fluctuates around a single value) to a collective period-two state (a state for which the time series of h_t alternatively moves between the corresponding neighborhoods of two separated values). Increasing the coupling induces the emergence of collective states of higher periodicity. Figure 6(b) shows that global attractors of period 2, 4 and 8 are possible in this globally coupled map system.

Figure 4 indicates the region in the phase diagram of the system where collective periodic behaviors occur. No quasiperiodic or more complex collective dynamics have been found in this region of parameters. This has been verified by looking at the time series of h_t or its return map. We have also checked system-size effects: when the lattice size N is increased the segments in the bifurcation diagrams such as fig. 6 shrink, indicating that the global periodic attractors become better defined in the large system limit. Collective quasiperiodic orbits, instead, reach a finite size with increasing N [6]. As a comparison, global quasiperiodic behavior is a common feature in globally coupled systems of unimodal or bounded maps [13–16].

The amplitudes of the collective periodic motions manifested in the mean field h_t do not decrease with increasing the system size N. As a consequence, the variance of the fluctuations of h_t itself does not decrease as N^{-1} with increasing N, but it saturates at some constant value related to the amplitude of the collective period. This is a phenomenon of nontrivial collective behavior, where macroscopic quantities on a system of nonlinear elements show a regular temporal evolution in spite of the presence of local chaos [5].

The dynamics of the collective periodic states is related to the existence of unstable periodic orbits and to the dynamics of the iterates of the single logarithmic map on its chaotic range. Figure 7 shows the superposition of successive instantaneous distributions $P_t(x)$ of site variables $x_t(i)$ of the globally coupled system with parameters yielding collective period 4. The locations of the unstable orbits of periods 1 and 2 of the logarithmic map are also indicated. The distribution $P_t(x)$ vary periodically in time, with approximate period 4. The chaotic elements tend to move together and periodically around the unstable periodic orbits at successive time steps. The individual values may be different within each zone separated by the unstable periodic orbits. The resulting mean field oscillates with approximate period 4 around the unstable fixed point $\bar{x}_1$ and the unstable period 2 orbit $\bar{x}_a$, $\bar{x}_b$ (fig. 2), which establish "reference" lines for the organization of the collective periodic behavior. In the collective period 2 state, the oscillations of the distribution $P_t(x)$ and the mean field h_t occur alternatively about the unstable fixed point $\bar{x}_1$. Similarly, the observed collective period 8 arises from oscillations of the distributions $P_t(x)$ with approximate period 8 around the unstable orbits of periods 1, 2, and 4 of the local map in the region $b \in [-1, 1]$.

The collective periodic states reflect the dynamics of the iterates of the single logarithmic map in the given region of the local parameter b. These iterates tend to move in a certain sequence between the intervals limited by the unstable periodic orbits of the logarithmic map, but chaotically within each of these intervals, even though there are no gaps separating chaotic bands. In the region of the phase diagram corresponding to collective periodic behavior, coupling induces a weak synchronization in the network, in the sense that the time series of the local chaotic sites tend to move together around the local unstable periodic orbits as a single map does, but keeping some dispersion.

b) Collective chaotic bands.

As the parameters of the system approach their values on the synchronization boundary, the collective periodic attractors are destroyed, giving place to collective chaotic bands. Figure 8(a) shows the bifurcation diagram of h_t as a function of the coupling ϵ, with fixed value of the local parameter b in the chaotic range of the local maps. Random initial conditions are used for each value of ϵ in figs. 8(a) and 8(b).

Near the synchronization boundaries, the collective states described by the mean field take the form of chaotic bands which successively merge until complete synchronization is achieved. Figure 8(b) shows a magnification of the

bifurcation diagram of fig. 8(a) close to the lower synchronization boundary for the fixed value $b = -0.7$. There can be distinguished eight-band, four-band, two-band and single-band chaotic collective states. Adjacent to the synchronization boundaries in $b \in [-1, 1]$ lies the collective chaotic single-band state, corresponding to a swarm of chaotic elements which keep some coherence. Similar chaotic band structures are present along the the synchronization boundary in the region $b \in [-1, 1]$. Figure 4 shows the approximate location of the collective chaotic band states on the phase diagram of the system. The collective chaotic bands, as well as the collective periodic states, are manifestations of nontrivial collective behavior. In both cases, the fluctuations of the mean field h_t no not decrease as N^{-1} with increasing system size N.

The dynamics of the chaotic band states, as that of the collective periodic behavior manifested in h_t, is related to the presence of unstable periodic orbits in the chaotic interval of the local map (3). The values of the unstable fixed point and the unstable period two orbit corresponding to $b = -0.7$ are indicated in fig. 8(b) by horizontal lines. Figure 9 shows the successive instantaneous distributions $P_t(x)$ associated to the collective chaotic two-band state. The distribution $P_t(x)$ moves alternatively as a single group on each side of the unstable fixed point $\bar{x}_1$, but its motion is not periodic. In general, the elements of our globally coupled system Eq. (1) do not split into separate groups in order in order to produce either the observed collective chaotic band states or the collective periodic states. We attribute this behavior to the absence of separated chaotic bands in the dynamics of the local maps.

Figure 10(a) shows the return map of h_t at parameter values corresponding to the four-band state. The collective behavior comes from a global low-dimensional chaotic attractor. Figure 10(b) shows the structure of the lower portion of this global chaotic attractor. No quasiperiodic collective motion appears to take place. In fact, no form of quasiperiodic or more complex collective dynamics have been found in the phase diagram of this system of globally coupled logarithmic maps.

c) Full turbulence.

In figures 6 and 8, we can see the presence of collective fixed point states in the region $b \in [-1, 1]$. Actually, these states exist for parameter values outside of the synchronization boundaries, as figure 11 shows. In these ranges of parameters, the mean field h_t is the result of the superposition of N completely desynchronized and uncorrelated chaotic elements.

The time series of the mean field corresponding to these states fluctuates about a mean value. The variance (mean square deviation) of the time series does decrease as N^{-1} with increasing system size N, obeying a normal statistical behavior (the law of large numbers). We have verified this behavior up to size $N = 10^6$.

The collective fixed points correspond to fully turbulent states of the system, similar to the turbulent phase observed by Kaneko in globally coupled tent maps [17].

Figure 4 indicates the region on the space of parameters of the globally coupled system Eq. (1) where the collective turbulent states have been found.

V. SYSTEM SIZE EFFECTS.

Finally, we investigate the influence of the size of the network on the emergence of the different types of collective states observed in the globally coupled system, Eq. (1). Figures 12(a) and 12(b) show the asymptotic mean field h_t as a function of the system size N, for different parameter values corresponding to collective period-four behavior and collective chaotic two-band state, respectively. In each case, there is a different critical size of the system N_c at which the corresponding nontrivial collective behavior distinctively emerges, i.e., $N_c \approx 25$ for the two-band state, and $N_c \approx 450$ for the period-four state. The smaller value of N_c for the two-band state is related to the greater synchronization of this state with respect to the period-four state (fig. 5). Note that the synchronized states are independent of N, i.e., $N_c \to 0$. The critical system size for the onset of collective states tends to increase as the parameter values move away from the synchronization boundary.

VI. CONCLUSIONS.

The collective behavior of a system of globally coupled logarithmic maps has been investigated on its space of parameters. We have found different collective states on the phase diagram of the system, corresponding to synchronized and to desynchronized states. The later correspond to nontrivial collective behaviors, consisting of collective

periodicity and banded chaos, and to full turbulence. The critical size of the system for the onset of collective behavior varies for the different states. The global states are reminiscent of thermodynamical phases, characterized by statistical quantities such as the mean field or the mean standard deviation, which may act as order parameters.

We have noted that the dynamics of the collective periodic states and that of the collective chaotic bands are related to the unstable periodic orbits and to the the dynamics of the isolated logarithmic map. Coupling can induce a global ordered motion around the unstable periodic orbits of the local map. In the other hand, the presence of periodic windows in the local dynamics does not seem determinant for the emergence of ordered collective behavior in systems globally coupled maps, as it has been argued recently [24]. The properties of the logarithmic map are quite different from those of previously used local dynamics in the context of globally coupled maps. The corresponding emergent collective states are also different. No clustering, no splitting of the elements in distinct groups, nor quasiperiodicity or more complex collective behaviors appear to take place in our model. Instead, those features are commonly observed in the collective dynamics of globally coupled maps belonging to standard universality clases (quadratic, circle or tent maps). Recent studies of globally coupled "chaotic singular maps" (a class to which the logarithmic map belongs) have shown that the corresponding collective states are similar to those found in the present system [20].

Much effort has been dedicated to establishing the necessary conditions for the emergence of nontrivial collective behaviors in lattices of nonlinear coupled elements, mostly involving numerical simulations. The observation of ordered collective behaviors in the present system, where the local dynamics has very specific properties, suggests that this kind of collective behavior should be a rather common phenomenon in deterministic systems of globally coupled chaotic elements.

The existence of unstable periodic orbits in the local maps is a relevant factor for the organization of nontrivial collective behavior. Our results suggest that the characteristics of the collective behaviors that emerge in globally coupled systems, are determined by general properties of the local elements, such as their universality class.

ACKNOWLEDGMENTS

We thank Prof. A. Parravano for useful discussions. This work was supported in part by a grant from Consejo de Desarrollo Científico, Humanístico y Tecnológico, and calculations were performed at the Centro Nacional de Cáculo Científico, both institutions of the Universidad de Los Andes, Mérida, Venezuela.

---

[1] K. Kaneko, *Physica D* **41**, 137 (1990).
[2] For recent surveys, see *Theory and Applications of Coupled Map Lattices*, edited by K. Kaneko, Wiley, N. Y., (1993); *Chaos* **2**, No. 3, focus issue on CML, (1992), edited by K. Kaneko.
[3] K. Kaneko, *Phys. Rev. Lett.* **65**, 1391 (1990).
[4] N. Chatterjee and N. Gupte, *Phys. Rev. E* **53**, 4457 (1996).
[5] H. Chaté, A. Lemaitre, P. Marq and P. Manneville, *Physica A* **224**, 447 (1996).
[6] H. Chaté and P. Manneville, *Europhys. Lett.* **17**,291 (1992); *Prog. Theor. Phys.* **87**, 1 (1992).
[7] P. M. Binder and V. Privman, *J. Phys. A* **25**, L775 (1992).
[8] P. Hadley and K. Wiesenfeld, *Phys. Rev. Lett.* **62**, 1335 (1989).
[9] K. Wiesenfeld, C. Bracikowski, G. James, and R. Roy, *Phys. Rev. Lett.* **65**, 1749 (1990).
[10] S. H. Strogatz, C. M. Marcus, R. M. Westervelt, and R. E. Mirollo, *Physica D* **36**, 23 (1989).
[11] N. Nakagawa and Y. Kuramoto, *Physica D* **75**, 74 (1994).
[12] K. Kaneko, *Physica D* **75**, 55 (1994); *Physica D* **77**, 456 (1994).
[13] K. Kaneko, *Physica D* **86**, 158 (1995).
[14] G. Perez, S. Sinha and H. A. Cerdeira, *Physica D* **63**, 341 (1993).
[15] K. Kaneko, *Physica D* **54**, 5 (1991).
[16] A. Pikovsky and J. Kurths, *Physica D* **76**, 411 (1994).
[17] K. Kaneko, *Physica D* **55**, 368 (1992).
[18] T. Kawabe and Y. Kondo, *Prog. Theor. Phys.* **85**, 759 (1991).
[19] M. G. Cosenza, *Phys. Lett. A*, **204**, 128 (1995).
[20] M. G. Cosenza and O. Alvarez-Llamoza, *unpublished.*
[21] I. Waller and R. Kapral, *Phys. Rev. A* **30**, (1984) 2047.
[22] Z. Neufeld and T. Viseck, *J. Phys. A* **28**, 5257 (1995).

[23] F. Xie and G. Hu, *Clustering dynamics in globally coupled map lattices*, preprint chao-dyn/9701001 (1997).
[24] T. Shinbrot, *Phys. Rev. E* **50**, 3230 (1994).

FIG. 1. Bifurcation diagram of the logarithmic map Eq. (3) as a function of the parameter b. For each value of b, 100 iterates are plotted after discarding 1000 transients.

FIG. 2. Some unstable periodic orbits of the logarithmic map, indicated by dotted lines, as a function of the parameter b. The stable fixed points x_1^* and x_2^* are plotted with solid lines. $\bar{x}_1$: unstable fixed point arising from x_1^*; $\bar{x}_a$, $\bar{x}_b$: unstable period two orbit, $f(\bar{x}_a) = f(\bar{x}_b)$.

FIG. 3. Lyapunov exponent for the logarithmic map as a function of the parameter b, calculated over 5×10^4 iterates after neglecting 5000 transients for each value of b.

FIG. 4. Phase diagram of the system Eq. (1). The synchronization boundaries are indicated by thick lines. The ± 1 labels on each curve identify the corresponding sign in Eqs.(6) and (7). The regions of parameters where the different collective states occur are identified. CPB: collective periodic behavior; CCB: collective chaotic bands; fully turbulent states are also located.

FIG. 5. Mean standard deviation $\langle \sigma \rangle$ vs. the coupling parameter ϵ, with fixed $b = -0.7$. System size $N = 10^5$; $\langle \sigma \rangle$ was calculated over 5000 iterations of the system Eq. (1), after discarding 2000 transients. The zones corresponding to the different collective states in this diagram are indicated with a notation similar to fig. 4

FIG. 6. Bifurcation diagram of the mean field h_t as a function of the parameter b for two different values of the coupling. $N = 10^5$. a) $\epsilon = 0.2$; b) $\epsilon = 0.25$.

FIG. 7. Superposition of 16 successive distributions $P_t(x)$ corresponding to collective period-four behavior, after transients. The locations of the unstable fixed point $\bar{x}_1$ and unstable period-two orbits $\bar{x}_a$, $\bar{x}_b$ are shown. $N = 10^5$, $b = -0.7$, $\epsilon = 0.24$. The numbers beside the distributions indicate the order in which they occur.

FIG. 8. a) Bifurcation diagram of the mean field h_t as a function of the coupling ϵ, with fixed $b = -0.7$ and $N = 10^5$. b) Magnification of the left part of a); the horizontal lines indicate the value of the unstable fixed point $\bar{x}_1$ and the values of the unstable period-two orbit on each side of $\bar{x}_1$, for the logarithmic map with $b = -0.7$. The vertical lines correspond to the approximate boundaries of different collective states which are indicated; S: synchronized state, CCB: collective chaotic bands; CPB: collective periodic behavior.

FIG. 9. Superposition of 8 successive distributions $P_t(x)$ for parameter values $b = -0.7$, $\epsilon = 0.276$, corresponding to a collective chaotic two-band state, after transients. Distributions corresponding to odd (even) time steps fall to the left (right) of $\bar{x}_1$, respectively. System size $N = 10^5$.

FIG. 10. a) Return map of the mean field h_t corresponding to a collective chaotic four-band state, $b = -0.7$, $\epsilon = 0.265$; $N = 10^5$. 8000 iterates are shown, after transients. b) Magnification of the lower part of a).

FIG. 11. Bifurcation diagram of h_t vs. b for two different values of ϵ, corresponding to fully turbulent states.

FIG. 12. Bifurcation diagram of h_t as a function of the system size N, corresponding to different collective states. a) collective period-four, $b = -0.7$, $\epsilon = 0.24$; b) collective chaotic two-band, $b = -0.7$, $\epsilon = 0.276$.

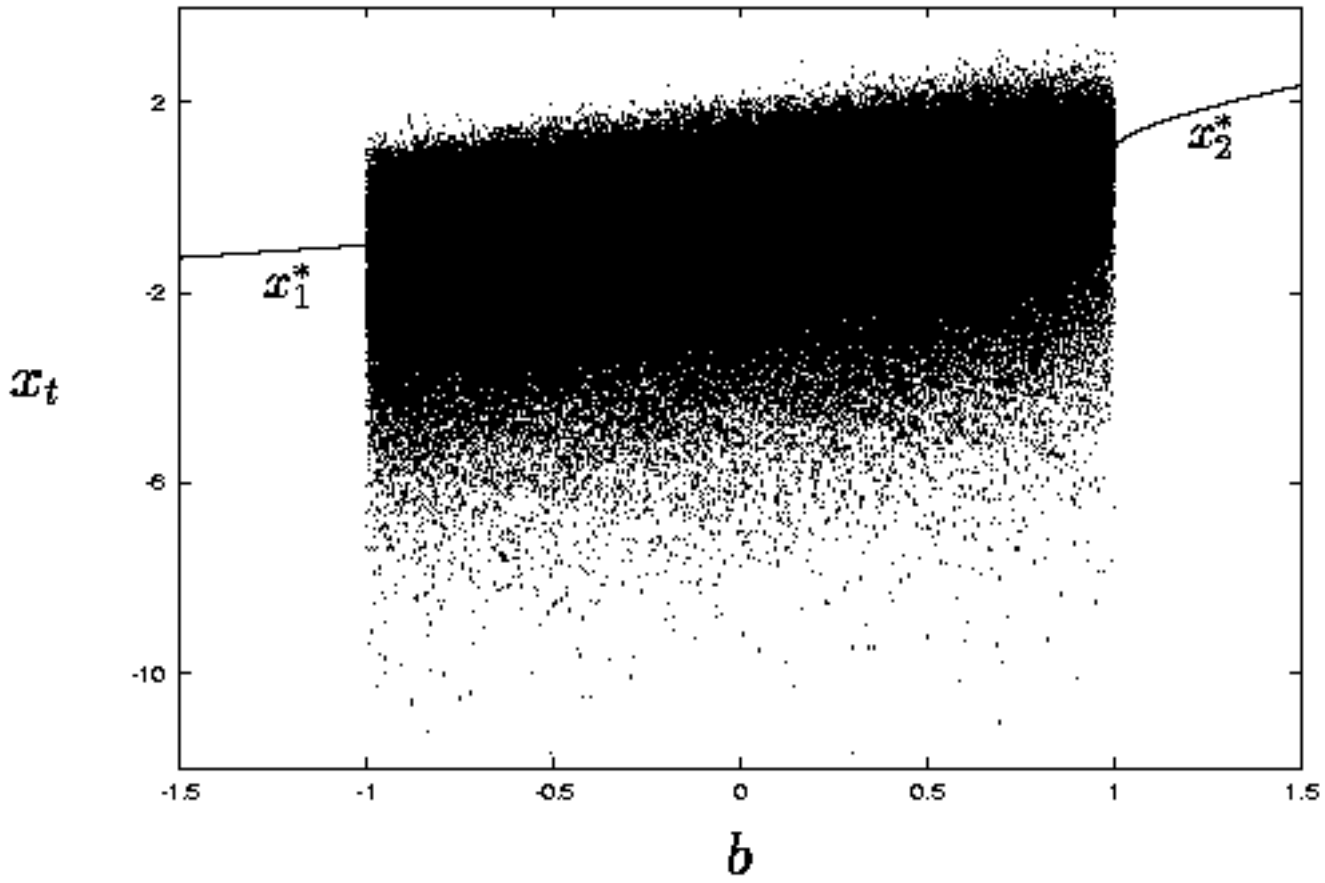

Figure 1

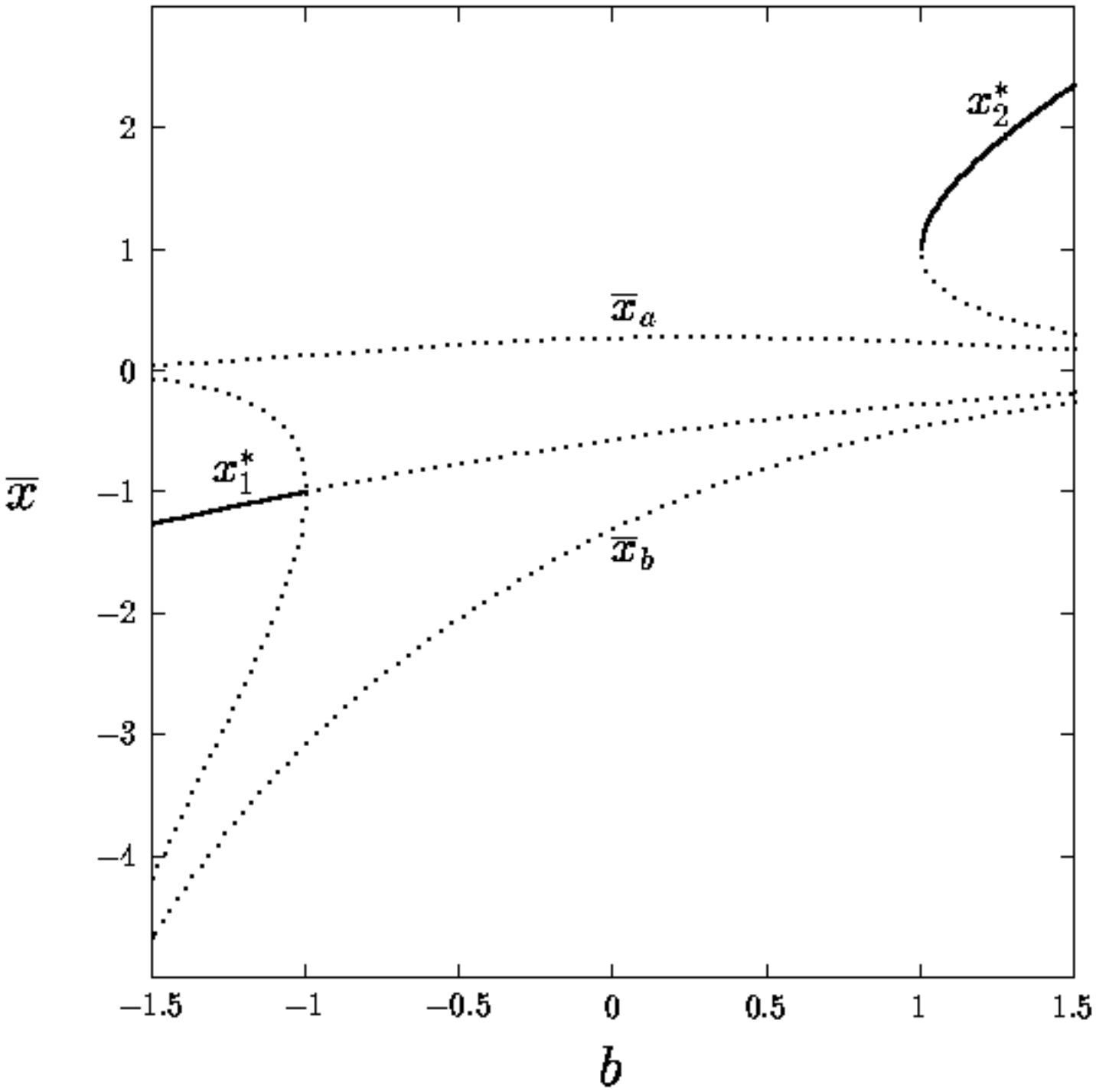
x_2^*
$\overline{x}_a$
x_1^*
$\overline{x}_b$
$\overline{x}$
b
2
1
0
−1
−2
−3
−4
−1.5
−1
−0.5
0
0.5
1
1.5

Figure 2

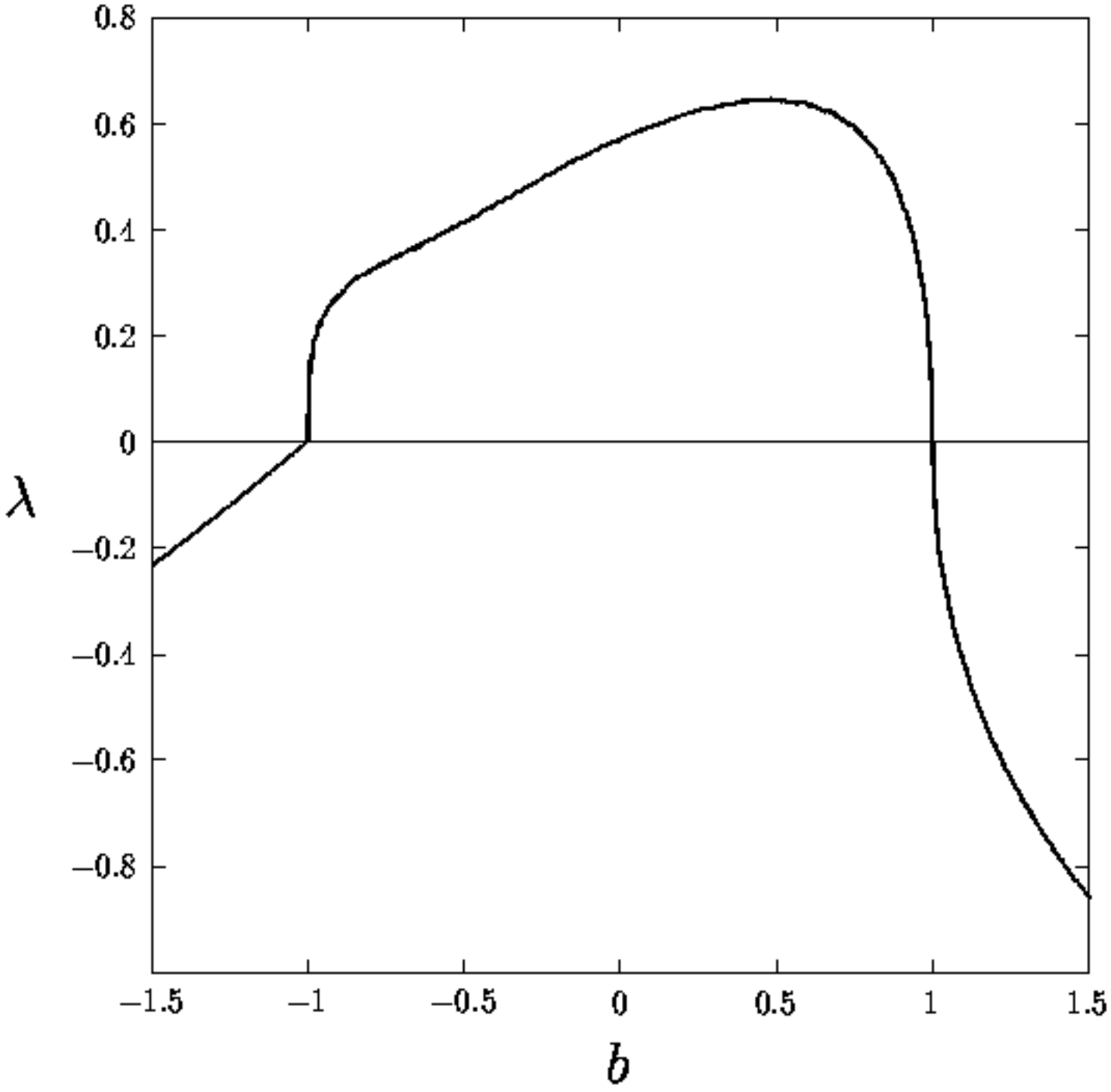

Figure 3

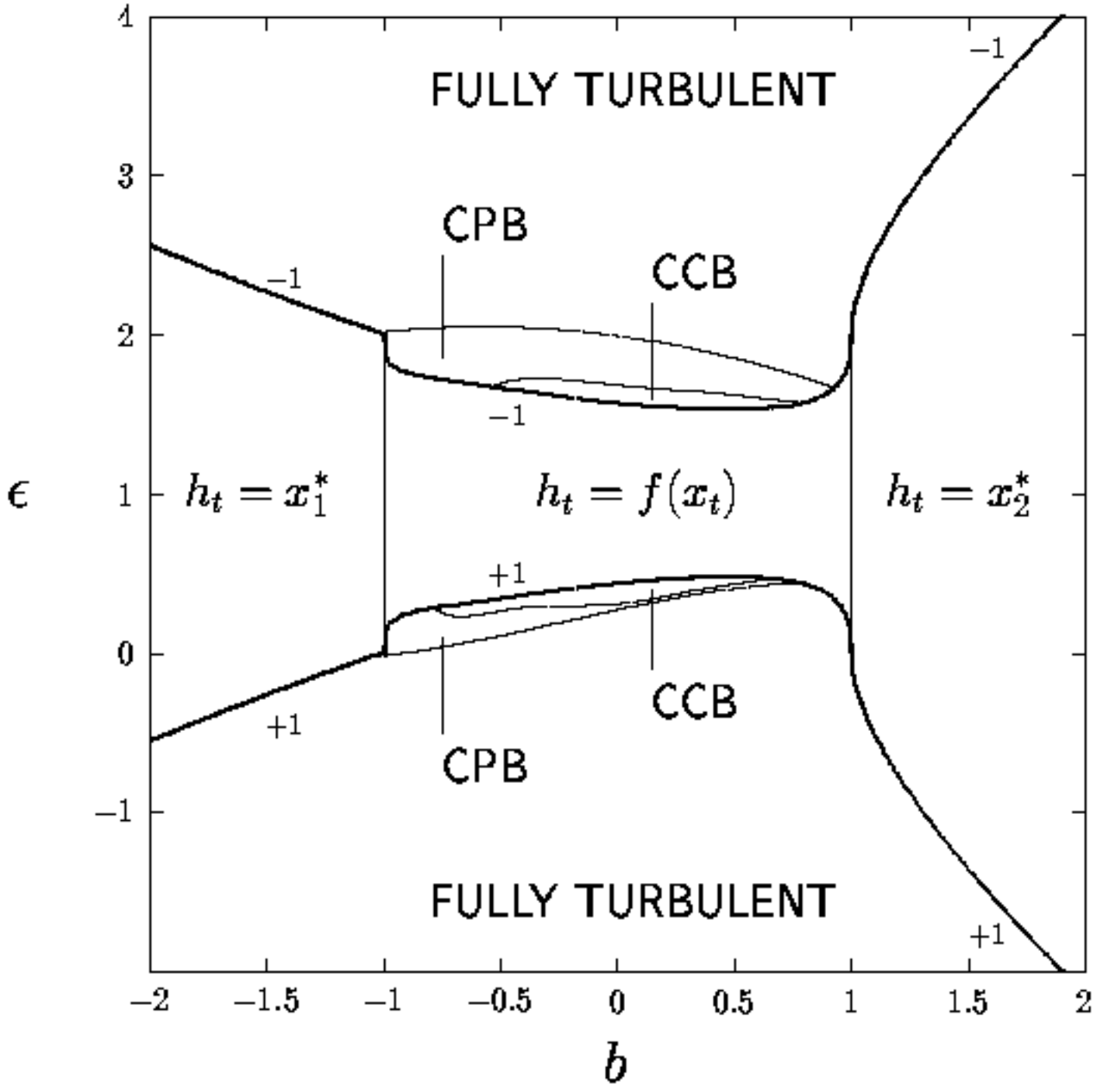
FULLY TURBULENT
CPB
CCB
−1
−1
−1
$h_t = x_1^*$
$h_t = f(x_t)$
$h_t = x_2^*$
+1
+1
CCB
CPB
FULLY TURBULENT
+1
ϵ
b
4
3
2
1
0
−1
−2
−1.5
−1
−0.5
0
0.5
1
1.5
2

Figure 4

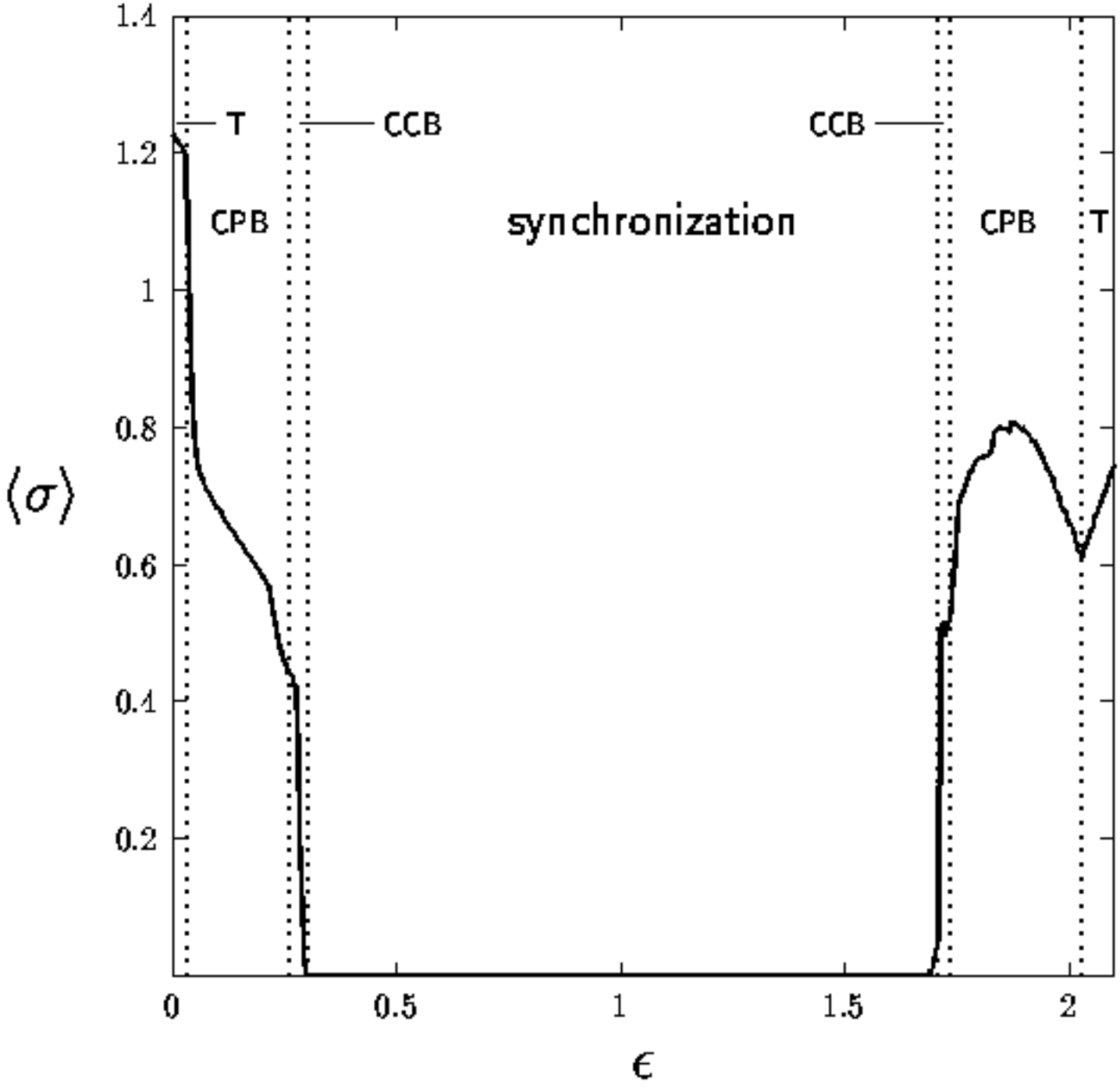
1.4
1.2
1
0.8
0.6
0.4
0.2
0
0.5
1
1.5
2
⟨σ⟩
ϵ
T
CCB
CCB
CPB
synchronization
CPB
T

Figure 5

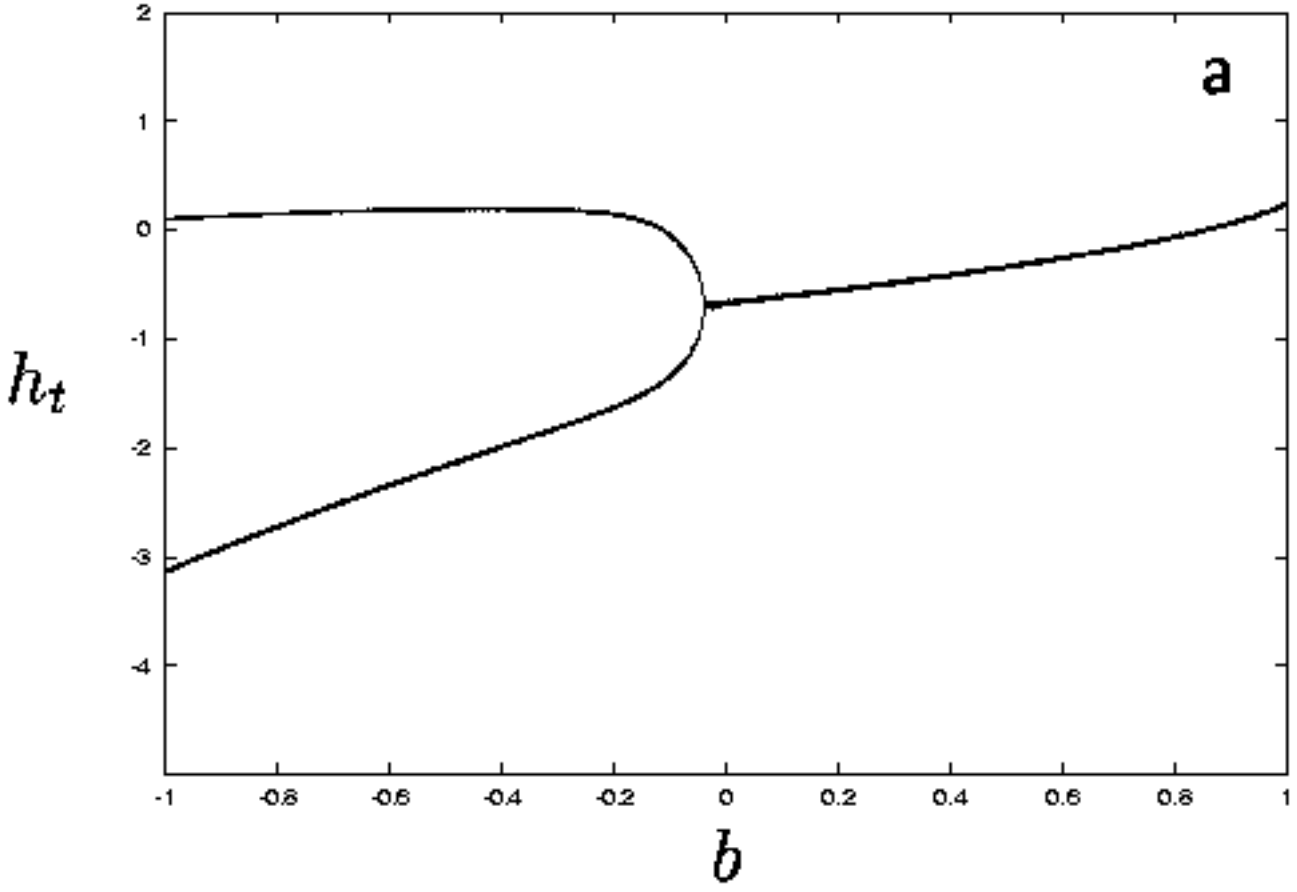

Figure 6 (a)

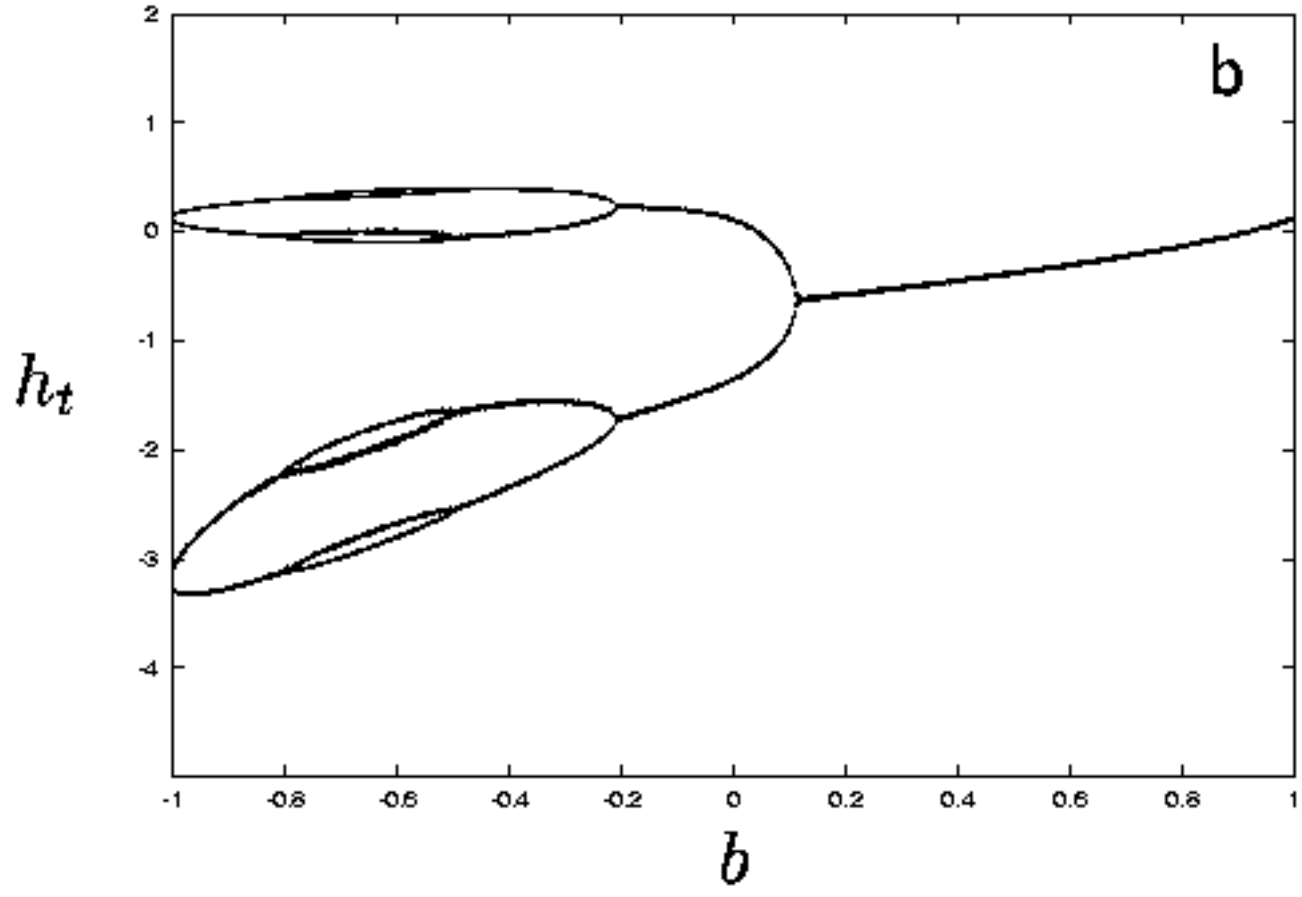

Figure 6 (b)

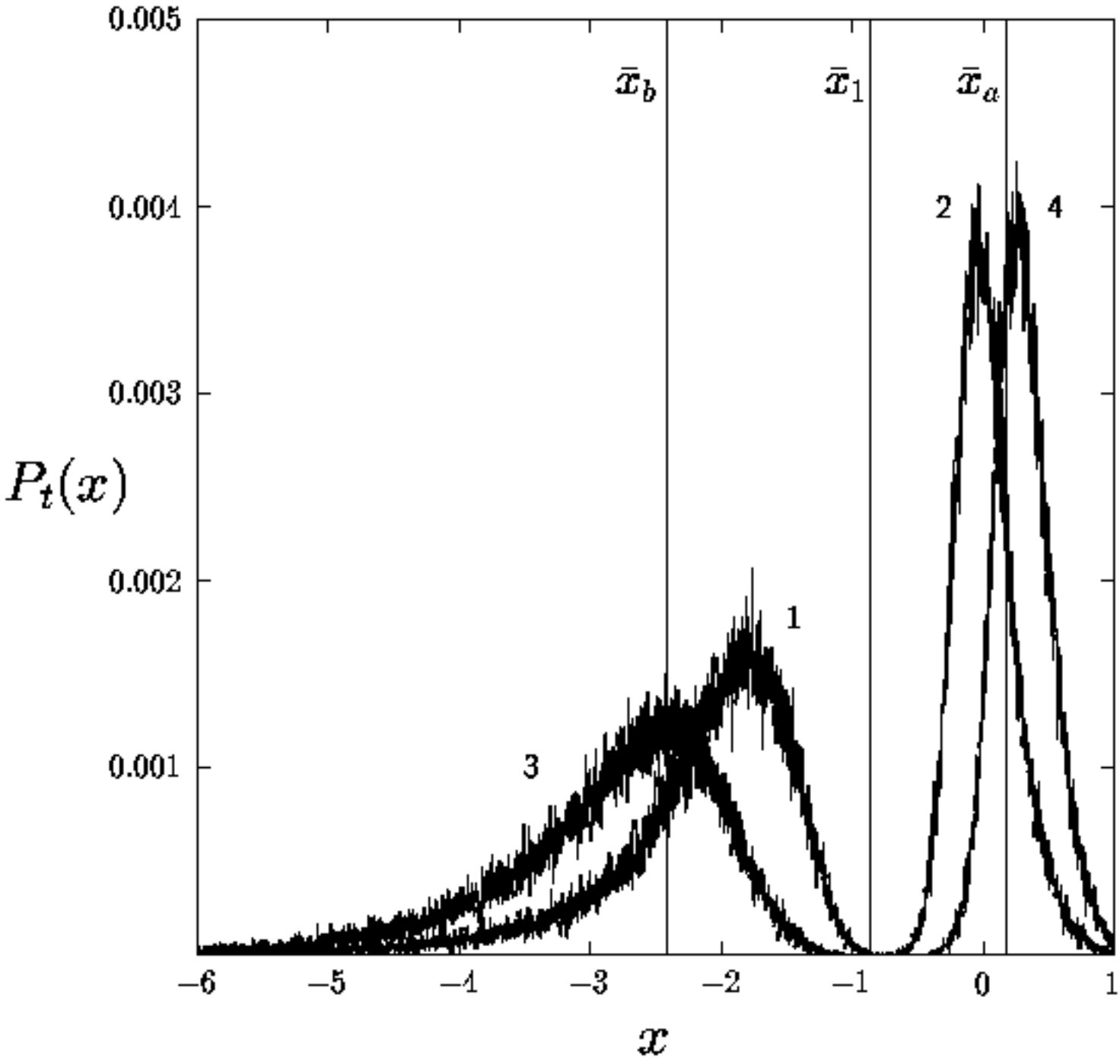
0.005
0.004
0.003
0.002
0.001
$P_t(x)$
$\bar{x}_b$
$\bar{x}_1$
$\bar{x}_a$
1
2
3
4
−6
−5
−4
−3
−2
−1
0
1
x

Figure 7

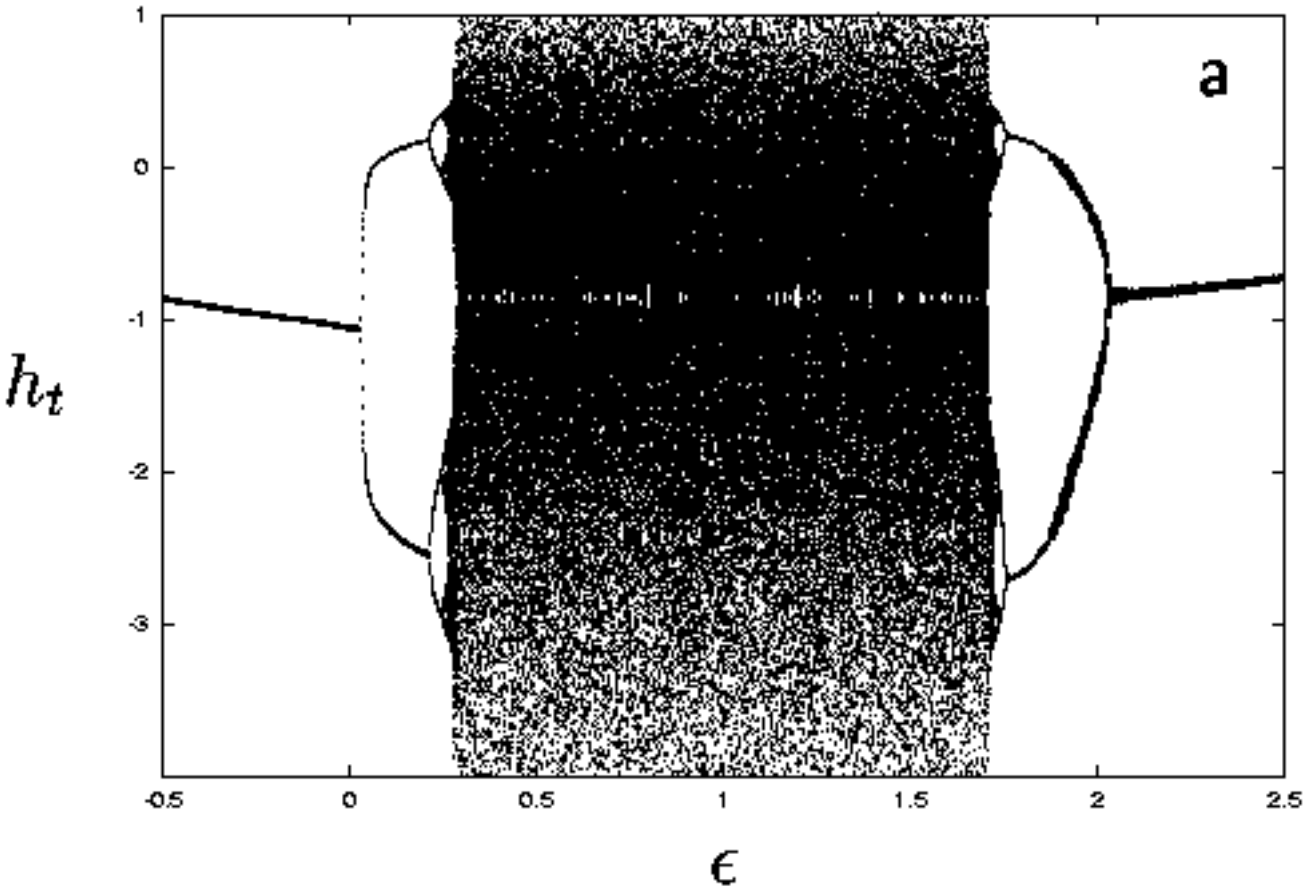

Figure 8 (a)

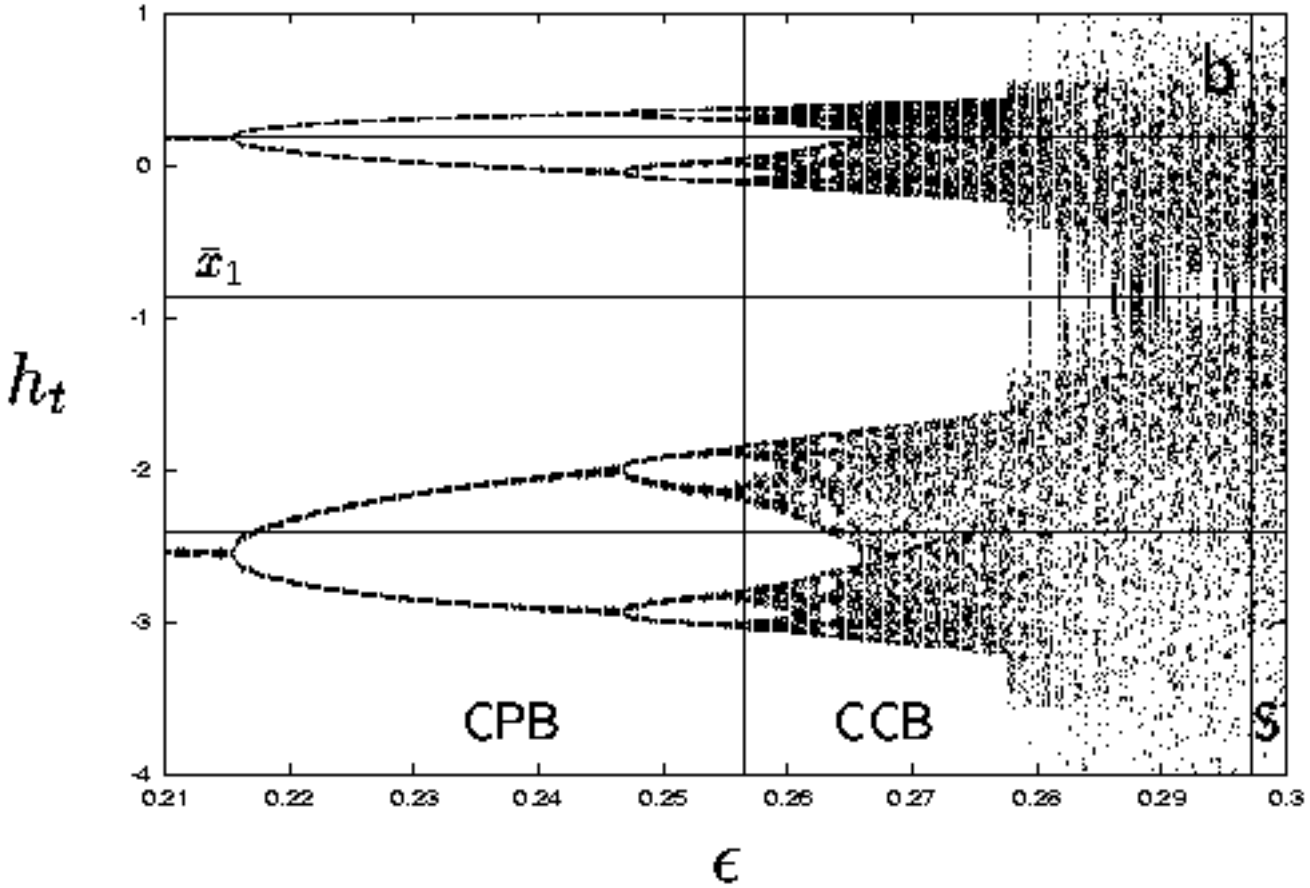

Figure 8 (b)

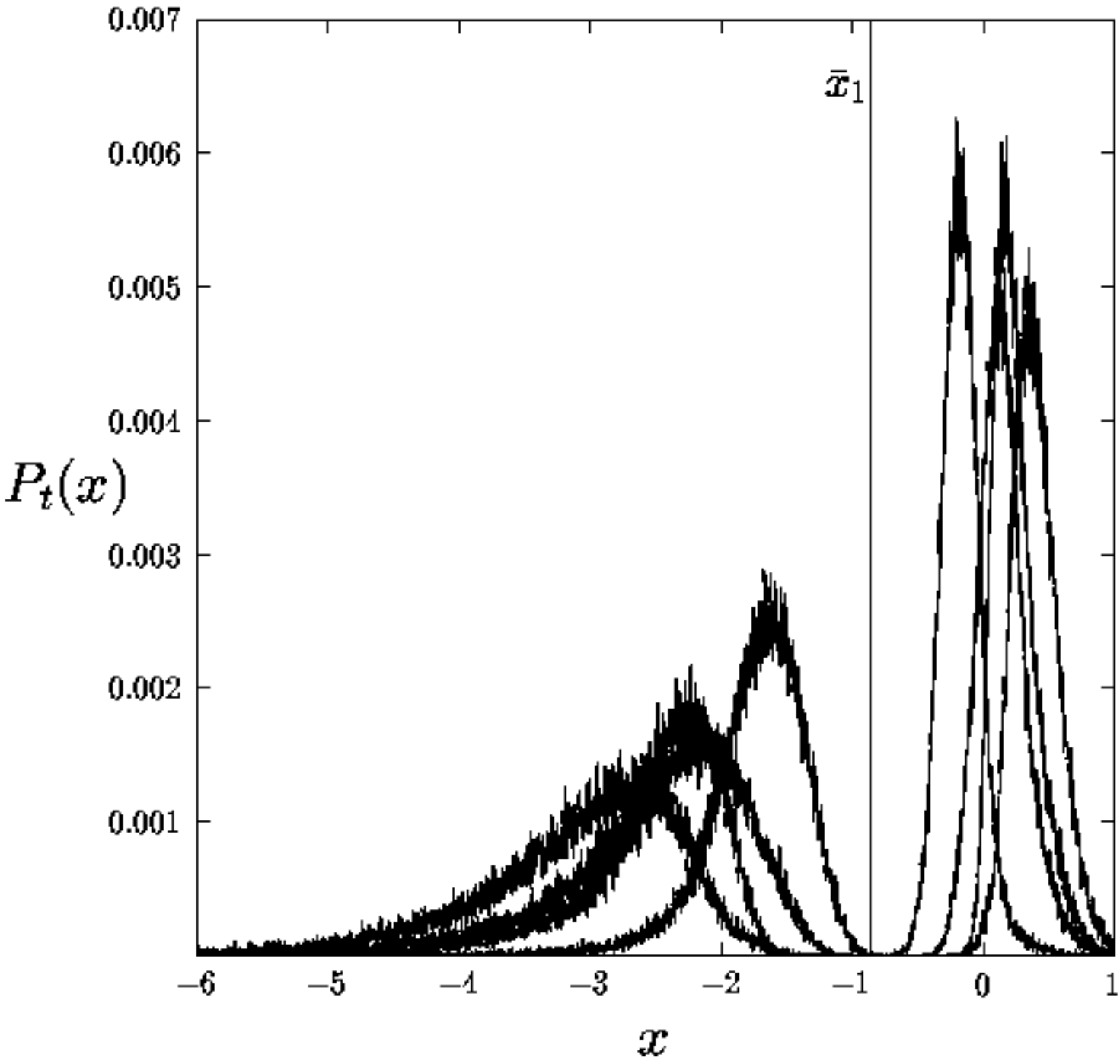

Figure 9

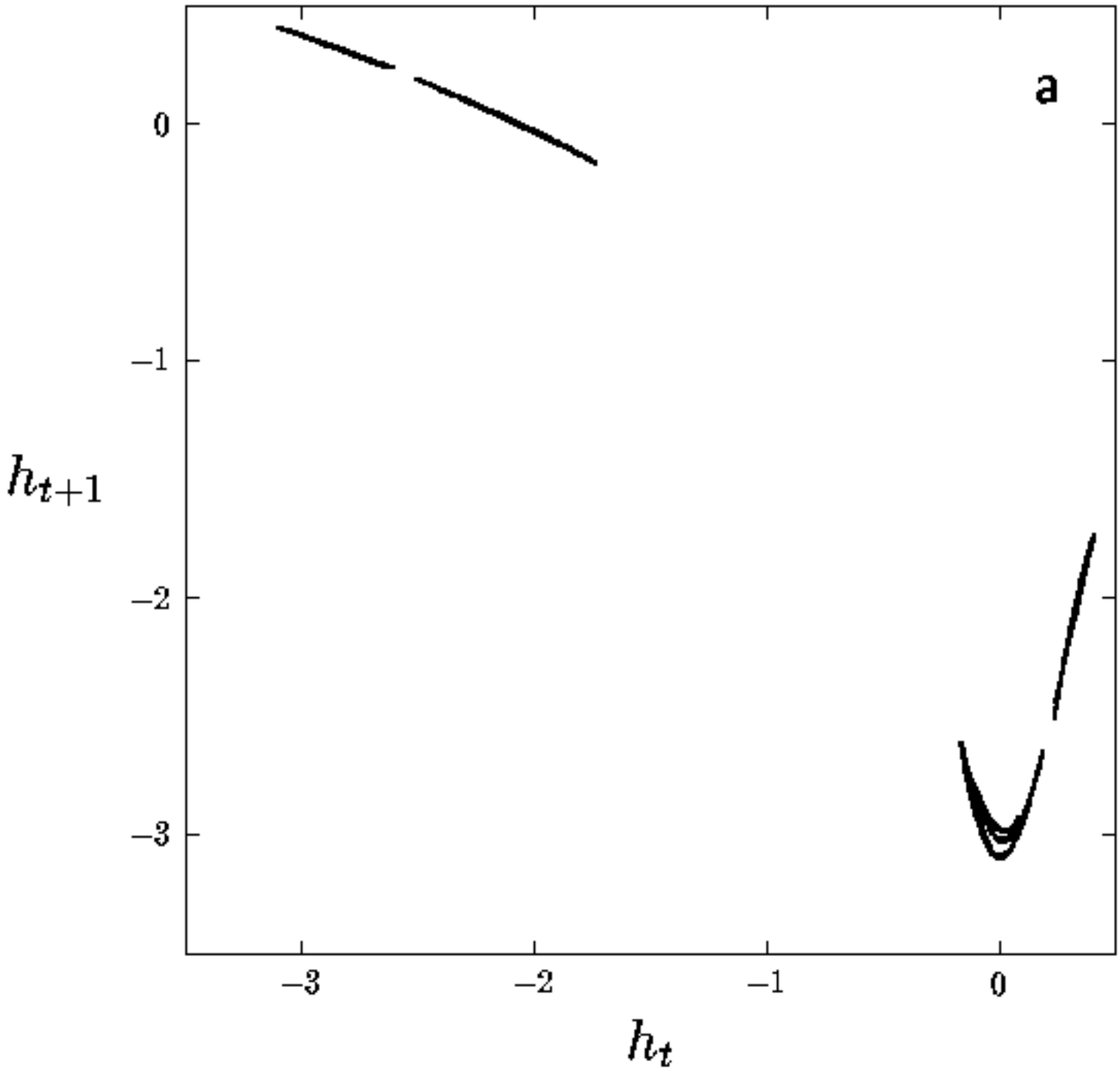

Figure 10 (a)

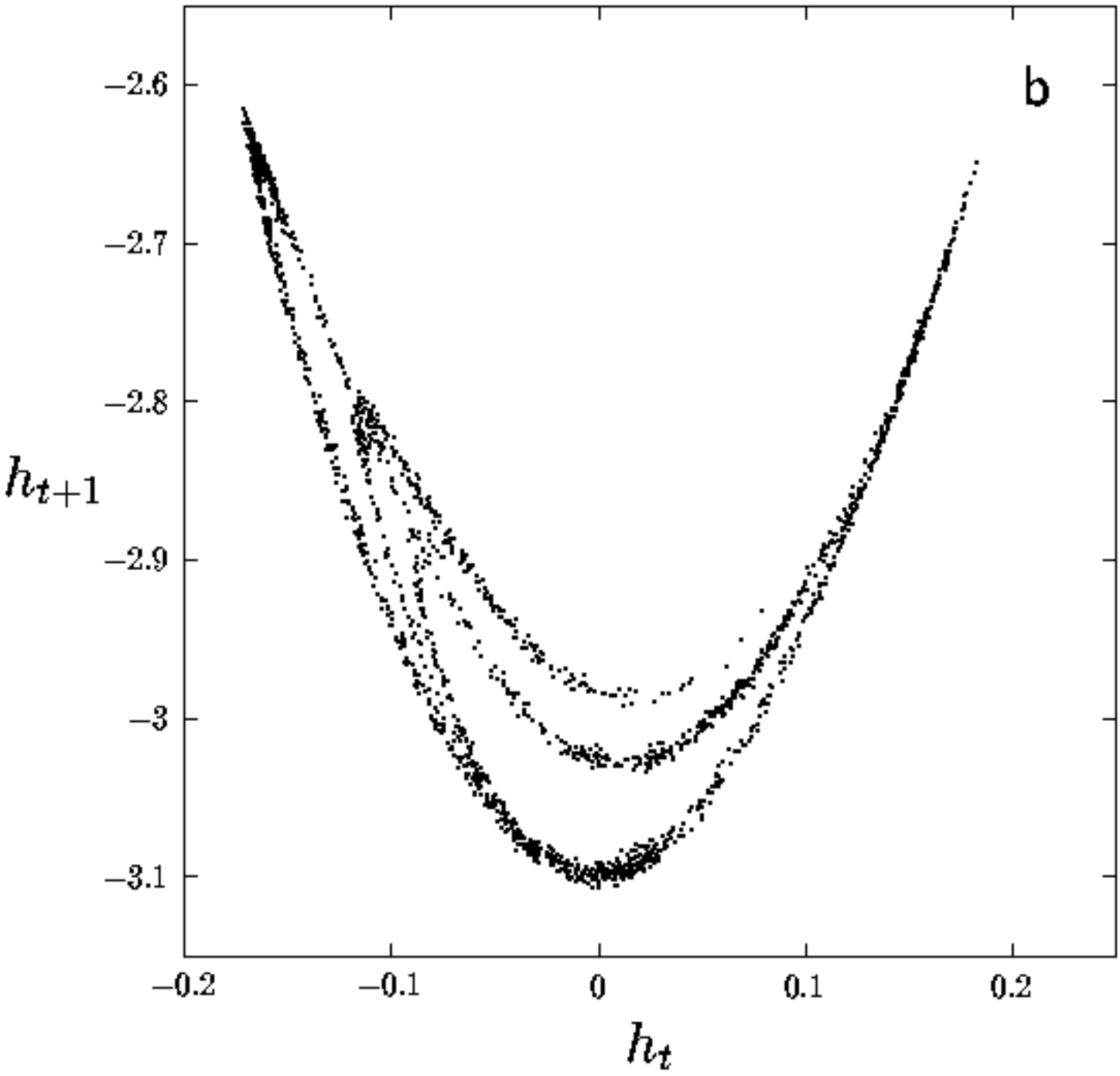

Figure 10 (b)

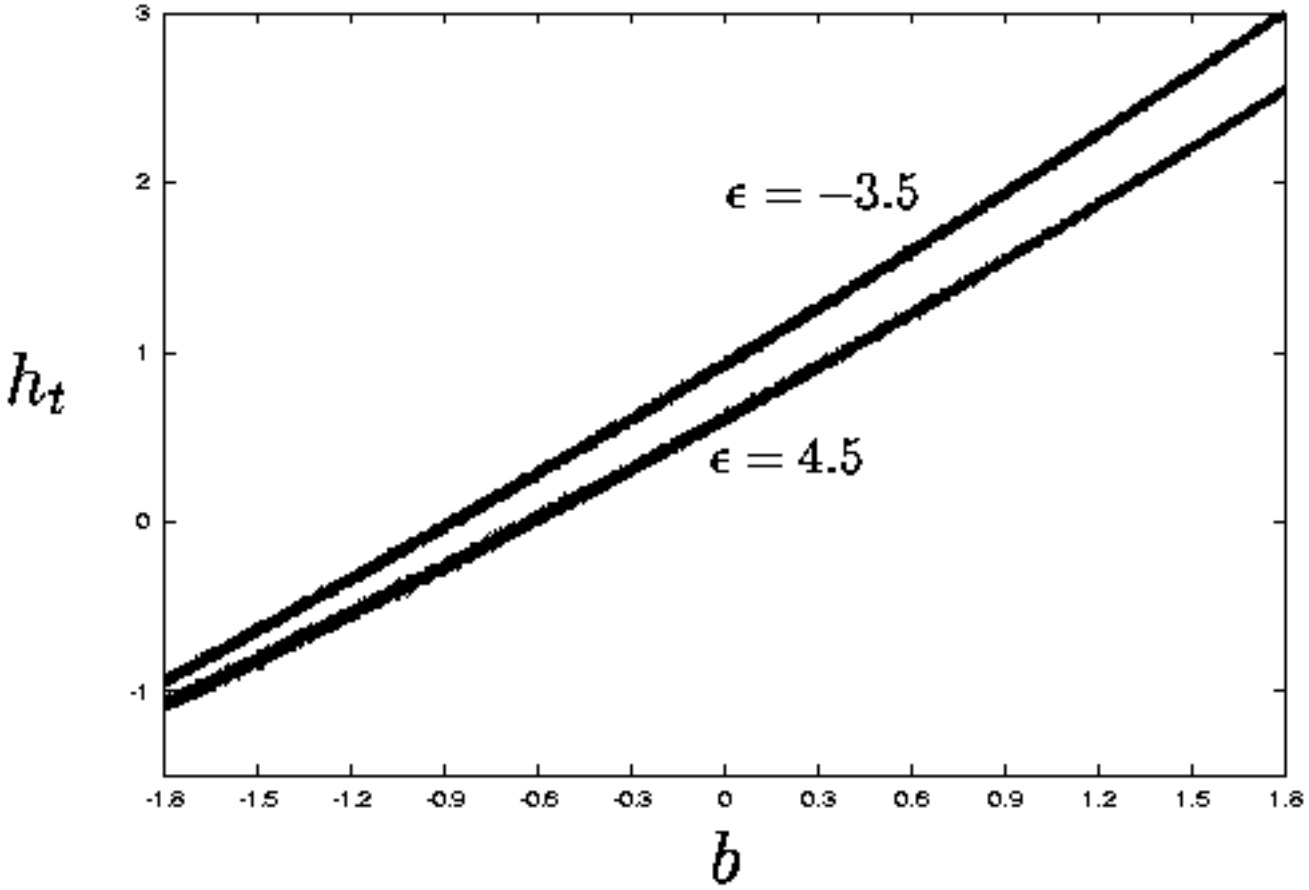
h_t
3
2
1
0
-1
$\epsilon = -3.5$
$\epsilon = 4.5$
-1.8
-1.5
-1.2
-0.9
-0.6
-0.3
0
0.3
0.6
0.9
1.2
1.5
1.8
b

Figure 11

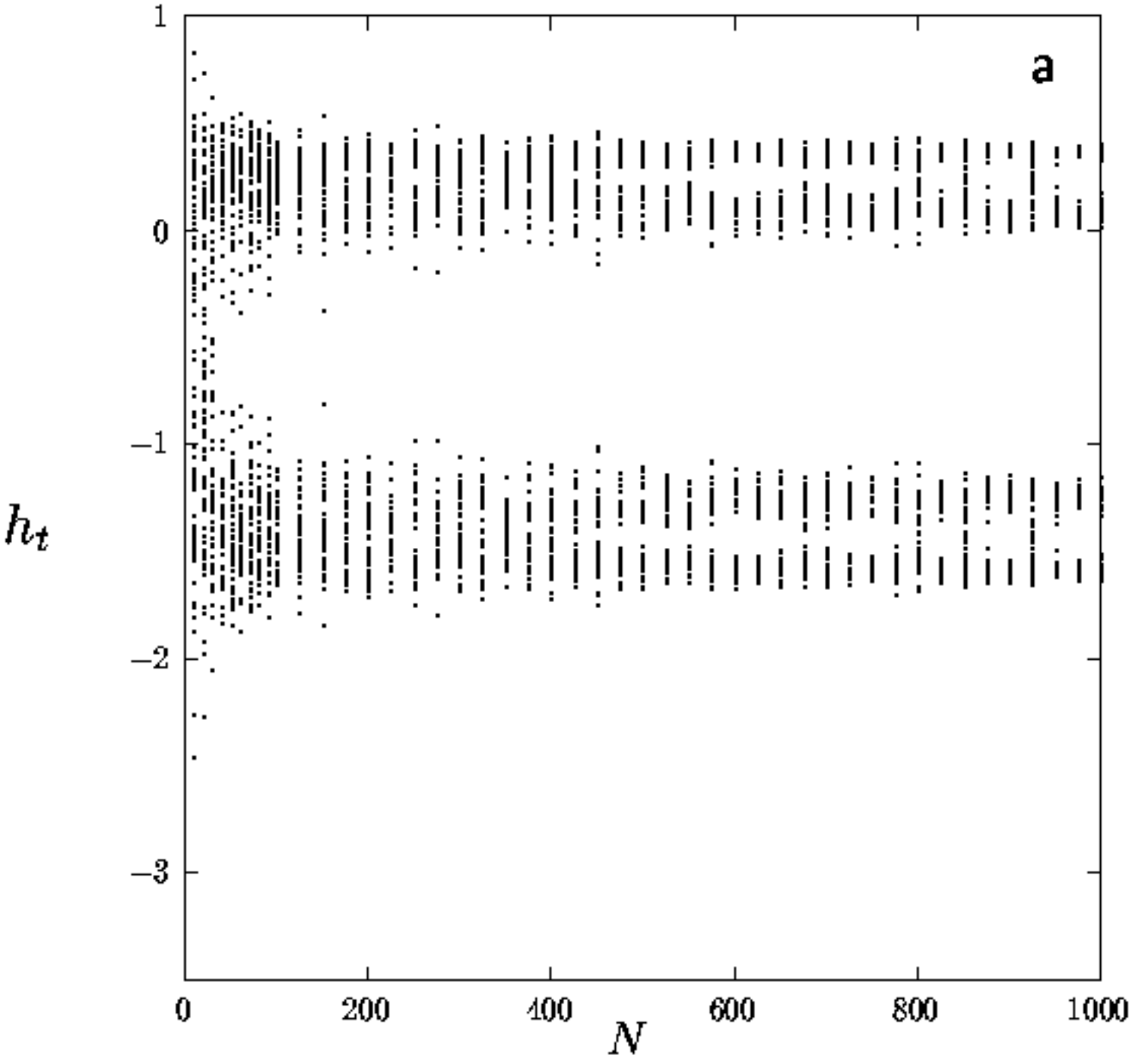

Figure 12 (a)

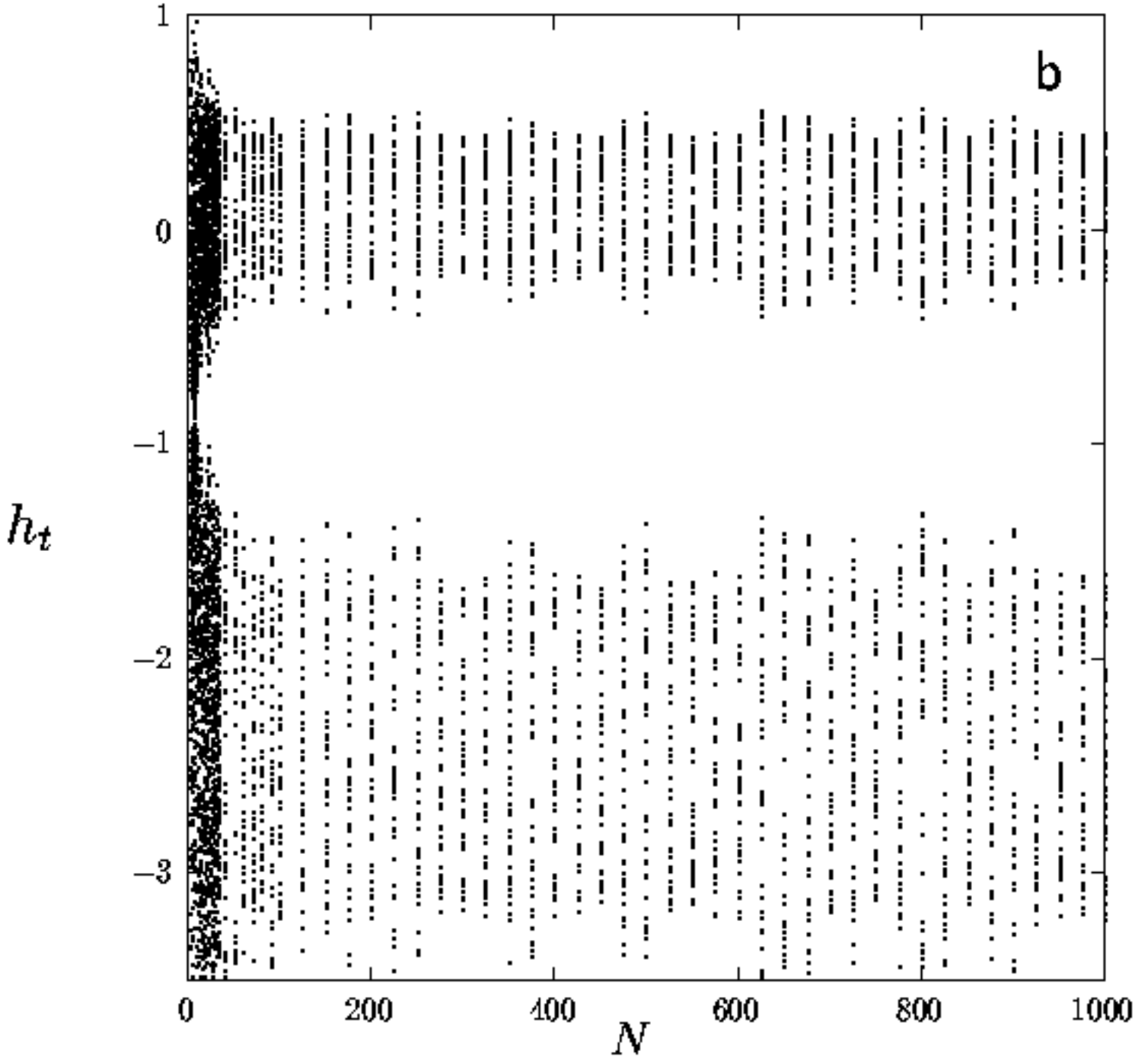

Figure 12 (b)